Characterization and Electrocatalytic Behavior of Layered Li_2MnO_3 and Its Acid-Treated Form

J. Katana Ngala,[†] Shaun Alia,[†] Arthur Dobley,[‡] Vincent Mark B. Crisostomo,[†] and Steven L. Suib*,[†]

Department of Chemistry, University of Connecticut, 55 North Eagleville Road, Unit 3060, Storrs, Connecticut 06269, and Lithion Inc., 82 Mechanic Street, Pawcatuck, Connecticut 06379

Received July 20, 2006. Revised Manuscript Received November 9, 2006

The material $H[H_{0.18}Li_{0.15}Mn_{0.67}]O_{1.90}$, obtained by the delithiation of layered Li_2MnO_3 using acid, gives a 2-fold increase in oxygen reduction ability versus Li_2MnO_3. Using elemental analysis by the ICP technique, average oxidation state determination, acid−base titrations, and thermal analysis, we determined the chemical composition of the proton-exchanged material to be $H[H_{0.18}Li_{0.15}Mn_{0.67}]O_{1.90}$. Rietveld refinement shows that the structure of the delithiated material is a monoclinic distortion of the *P*3 structure resulting in the *C*2/*m* space group with cell parameters $a = 5.049(2)$ Å, $b = 8.707(2)$ Å, $c = 4.903(1)$ Å, $\beta = 109.17(2)°$. The BET surface area for the materials increases from 18 to 57 m^2/g upon delithiation. Application of $H[H_{0.18}Li_{0.15}Mn_{0.67}]O_{1.90}$ as an electrocatalyst in a lithium-air cell gives a specific discharge capacity of 1618 mA h g^{-1}.

Introduction

There is a large amount of interest in improving the O_2 reduction efficiency of electrocatalysts for metal-air batteries and fuel cells. In principle, the reaction between the anode material and oxygen cathode in these types of cells is limited only by the amount of anode because O_2 is in large abundance. Thus, such types of cells give high discharge capacities. For instance, the Li-air battery is promising as a high-energy density source.

The electrocatalyst used to accelerate O_2 reduction in the cell is key in determining the electrical discharge by the cell, because O_2 reduction is the slower of the two half-reactions for the cell. The noble metal Pt, in nanoparticulate form, has excellent performance as an oxygen reduction electrocatalyst in fuel cells but is very expensive for large-scale application and, in addition, experiences poisoning.[1] Transition metal oxides have been widely investigated as alternatives to Pt and have shown a lot of potential as electrocatalysts.[2−6]

Manganese oxides have been widely studied not only as cathodes for both primary and secondary batteries but also as electrocatalysts for metal-air batteries.[1,7−13] Their application in these areas is due to the properties of a number of manganese oxide phases as intercalation hosts, which is appropriate for secondary battery applications, and as oxygen reduction catalysts for metal-air battery application. Both applications utilize the redox properties of Mn in oscillating between oxidation states. In addition, manganese oxides have the advantage of being inexpensive and environmentally friendly. Commercial Zn-air alkaline batteries, which have been widely used for more than five decades, employ manganese oxide as the electrocatalyst.[1]

There are a number of factors that determine the performance of an O_2 reduction catalyst. Surface area, metal oxidation state, electrical conductivity, structural distortions, oxygen vacancies, porosity, and the ability by the catalyst to decompose the reduction intermediate are key factors. Large surface areas provide a large number of active sites, which leads to high catalytic activity. The role of structural distortions was alluded to in explaining the electrocatalytic superiority of γ-MnOOH versus some other manganese oxide phases, as reported by Matsuki et al.[7] The role of oxygen vacancies is highlighted in the excellent catalyst RuO_2.[14] Oxygen vacancies in the structure result in lone electrons on some of the transition metal d orbitals. The lone electrons, also known as F centers, are available to be donated to adsorbed molecular O_2 on the catalyst surface. High porosity of the catalyst material allows better access of the O_2 to the

* To whom correspondence should be addressed. E-mail: steven.suib@uconn.edu.
† University of Connecticut.
‡ Lithion, Inc.

(1) Kinoshita, K. *Electrochemical Oxygen Technology*; Wiley: New York, 1992.
(2) Shimizu, Y.; Uemura, K.; Matsuda, H.; Miura, N.; Yamazoe, N. *J. Electrochem. Soc.* **1990**, *137*, 3430.
(3) Yamazoe, N.; Miura, N.; Shimizu, Y.; Uemura, K. *Prog. Batteries Sol. Cells* **1989**, *8*, 276.
(4) Manoharan, R.; Shukla, A. K. *Electrochim. Acta* **1985**, *30*, 205.
(5) Karlsson, G. *Electrochim. Acta* **1985**, *30*, 1555.
(6) Espinal, L.; Suib, S. L.; Rusling, J. *J. Am. Chem. Soc.* **2004**, *126*, 7676−7682.
(7) Matsuki, K.; Kamada, H. *Electrochim. Acta* **1986**, *31*, 13.
(8) Kanungo, S. B.; Parida, K. M.; Sant, B. R. *Electrochim. Acta* **1981**, *26*, 1157.
(9) Liompart, S.; Yu, L. T.; Mas, J. C.; Mendiboure, A.; Vignaud, R. *J. Electrochem. Soc.* **1990**, *137*, 371.
(10) Robertson, A. D.; Bruce, P. G. *Chem. Commun.* **2002**, *23*, 2790.
(11) Kalyani, P.; Chitra, S.; Mohan, T.; Gopukumar, S. *J. Power Sources* **1999**, *80*, 103.
(12) Paik, Y.; Grey, C. P.; Johnson, C. S.; Kim, J.-S.; Thackeray, M. M. *Chem. Mater.* **2002**, *14*, 5109.
(13) Jain, G.; Yang, J.; Balasubramanian, M.; Xu, J. J. *Chem. Mater.* **2005**, *17*, 3850−3860.
(14) Knapp, M.; Seitsonen, A. P.; Kim, Y. D.; Over, H. *J. Phys. Chem. B* **2004**, *108*, 14392−14397.

10.1021/cm0616937 CCC: $37.00 © 2007 American Chemical Society
Published on Web 12/29/2006

active sites besides increasing the number of active sites. The decomposition of the reduction intermediate acts to facilitate fast O_2 reduction. Manganese oxides, in general, readily decompose H_2O_2 into OH^- and H_2O.[8,9] Thus, they are likely to effect fast O_2 reduction.

Layered Li_2MnO_3 (or $Li[Li_{10.33}Mn_{0.67}]O_2$, where the atoms in the square brackets represent atoms in the main framework of the structure) has been extensively studied as a cathode material for lithium rechargeable batteries.[10−13] Lithium can be extracted from the structure by proton exchange using acid.[12] The extraction occurs, in sequence, initially from the interlayer sites, followed by Li, together with lattice O, from the transition metal oxide layers. During the Li extraction, phase transformation occurs through layer shearing, and a decrease in particle size results.[12] The presence of H-bonding in the new phase provides the stabilization energy to compensate for the energy requirement in layer shearing. Because of the reversible nature of the ion-exchange reaction and its stability toward Li^+ ion cycling, Li_2MnO_3 was studied for ion-exchange applications.[15] To the best of our knowledge, no report is available on the study of Li_2MnO_3 and its proton-exchanged forms (H^+ forms) as electrocatalysts for oxygen reduction. The increase in surface area accompanying Li extraction is expected to enhance the catalytic activity of these materials. Moreover, lattice O loss from the main framework during the second step of Li extraction may have an additional impact on the activity due to the presence of O vacancies. Thus, Li_2MnO_3 presents a useful precursor toward active catalysts.

The properties of the layered Li_2MnO_3 and its H^+ form as electrocatalysts for oxygen reduction are reported here. For simplification, the as-prepared compound Li_2MnO_3 will be abbreviated as LM and its H^+ form as HLM. The effects of surface area, acidity, and oxygen vacancies on their properties are investigated. Herein, we also compare the O_2 reduction abilities of the prepared materials with that of γ-MnOOH, an established electrocatalyst for metal-air batteries.

Experimental Section

The compound Li_2MnO_3 was prepared by solid-state reaction between γ-MnO_2 (Aldrich) and LiOH (Fischer Chemicals) as previously reported.[12] The solid precursors were used in a MnO_2: LiOH mole ratio of 1:2 and thoroughly ground in an agate mortar. The mixture was heated at 650 °C for 24 h. A brick red-colored solid was obtained.

Acid treatment of Li_2MnO_3 was performed at room temperature using 4 M H_2SO_4 to obtain the proton-exchanged material. About 3 g of the sample LM was stirred in 50 mL of the acid for about 22 h. The mixture was then filtered and the precipitate rinsed with deionized water. The obtained solid was dark-brown. The concentration of the H_2SO_4, before and after reactiion with the sample, was determined according to Vogel.[16] A primary standard solution of sodium tetraborate was used to titrate the acid. The extent of protonation was then determined by the difference of the determined concentrations. The compound γ-MnOOH was also prepared using a reflux method according to Ardizzone et al.[17]

Average oxidation state (AOS) determination was performed using potentiometric titrations.[18] The sample was initially digested with concentrated HCl to obtain a solution of Mn^{2+} and determine the total Mn content. Complete dissolution of the solid sample occurred, forming Mn^{2+} solution. The obtained solution was then titrated with standardized $KMnO_4$ solution in the presence of sodium pyrophosphate to determine the concentration of Mn according to the following equation.

$$MnO_4^-(aq) + 4Mn^{2+}(aq) + 15H_2P_2O_7^{2-}(aq) + 8H^+(aq) \rightarrow 5Mn(H_2P_2O_7)^{3-}(aq) + 4H_2O \quad (1)$$

The total MnO_2 content in the sample was determined by reacting the solid sample with excess $Fe[NH_4]_2(SO_4)_2$ solution under a N_2 atmosphere according to eq 2, followed by back-titration of the excess Fe^{2+} with standard $KMnO_4$ solution according to eq 3.

$$MnO_2(s) + 2Fe^{2+}(aq) + 4H^+(aq) \rightarrow 2Fe^{3+}(aq) + Mn^{2+}(aq) + 2H_2O \quad (2)$$

$$MnO_4^-(aq) + 5Fe^{2+}(aq) + 8H^+(aq) \rightarrow 5Fe^{3+}(aq) + Mn^{2+}(aq) + 4H_2O \quad (3)$$

The AOS was calculated from the total number of moles of oxygen in the compound. The number of moles of oxygen in the form of MnO was calculated by the difference as follows.

$$\text{moles of MnO} = \text{moles of } Mn^{2+} - \text{moles of } MnO_2$$

The AOS was then calculated on the basis of the total amount of charge due to oxygen in the compound.

The prepared samples were characterized by various techniques. Powder X-ray diffraction was performed using a Scintag XDS2000 diffractometer with a Cu Kα source equipped with a Ge detector. A 0.02 step in 2θ/count, beam voltage of 45 kV, and beam current of 40 mA were used. A slow step scan of 10 s exposure was used for refinement quality patterns. Sample morphologies were obtained using field emission scanning electron microscopy (FESEM) on a DSM 982 Gemini. Sample suspensions were prepared in 2-propanol and applied on Si wafers. Thermal analysis was performed using a Dupont 951 TGA system. About 10 mg of sample was loaded into a Pt sample pan. The ramping rate was set at 10 °C/min. Elemental analysis was performed using inductively coupled plasma−atomic emission spectroscopy (ICP−AES) on a TJA Iris.

Surface areas of the samples were studied using a Micromeritics ASAP 2010 system. Before acquiring nitrogen adsorption and desorption isotherms at 77 K, samples were outgassed at 150 °C under a vacuum for 12 h. Surface areas were determined by nitrogen adsorption data using Brunauer−Emmett−Teller (BET) methods.[19]

Oxygen reduction studies were conducted by cyclic voltammetry experiments. Gas-diffusion electrodes were prepared. Sample mixtures consisting of sample, carbon powder, and PTFE binder at a ratio of 10:10:80 by weight were made. The mixtures were suspended in water and sonicated. The suspensions were coated on XR 72 carbon papers. The cell set up consisted of the sample mixture as working electrode with an SCE as the reference and Pt as the counter electrode. The electrolytes were 1 M KOH and a 1

(15) Tang, W.; Kanoh, H.; Yang, X.; Ooi, K. *Chem. Mater.* **2000**, *12*, 3271−3279.
(16) Vogel, L. *Textbook of Quantitative Inorganic Analysis*, 4th ed.; Longman Group Ltd.: London, 1978; p 326.
(17) Ardizzone, S.; Bianchi, C. L.; Tirelli, D. *Colloids Surf., A* **1998**, *134*, 305−312.
(18) Glover, D.; Schumm, B., Jr.; Kozowa, A. *Handbook of Manganese Dioxides Battery Grade*; International Battery Materials Association: Cleveland, OH, 1989; pp 25−32.
(19) Brunauer, S.; Emmett, P. H.; Teller, E. *J. Am. Chem. Soc.* **1938**, 309.

M $LiPF_6$ in a 1:1:1 DMC:EMC:EC mixture. In a typical experiment, N_2 gas was purged through the cell for about 30 min followed by an initial scan. This was followed by 30 min of O_2 gas purge and another scan. The oxygen flow was maintained above the electrolyte during the scan to ensure saturation.

Results and Discussion

Chemical Composition. The chemical compositions of the samples LM and HLM were determined by AOS determination and elemental analysis. The determined AOS for Mn in the sample LM is 4+. Analysis of the sample by ICP gave a 2:1 Li:Mn ratio. Both data support the chemical formula Li_2MnO_3. The sample HLM gave an AOS of 3.7+ for Mn, which is in agreement with a previous report that protonation of Li_2MnO_3 resulted in a decrease in average oxidation state of Mn.[12] The decrease in AOS is indicative of loss of lattice O as lithia (Li_2O), accompanied by proton gain to give an oxygen-deficient compound. On the basis of the ICP and AOS data, we calculated the chemical formula for sample HLM to be $H[H_{0.18}Li_{0.15}Mn_{0.67}]O_{1.90}$ compared to the original $Li[Li_{0.33}Mn_{0.67}]O_2$. The amount of Li^+ and H^+ ions in a proton-exchanged structure was previously reported to be lower than the original amount of Li^+ ion before acid treatment.[12] However, in this case, the ICP and AOS data support these amounts being equal. The high concentration of acid used in the reaction competes with the H^+ exchange from the structure.

The H_2SO_4 that was used for the Li extraction was titrated with standard $Na_2B_4O_{10}$ solution, before and after its reaction with the as prepared sample, to determine the extent of proton exchange. The number of moles of exchanged H^+ ions determined from the acid−base titration is in good agreement with ICP data. The titrations showed that about 0.2 mol Li remained in the structure upon protonation using 4.0 M for 22 h, which is in agreement with the determined chemical formula. Thus, the analyses indicate that some of the Li from the main framework, in addition to the Li from the Li layers, was extracted. It is interesting to note that concentrated HCl, unlike H_2SO_4, causes the complete dissolution of Li_2MnO_3. This is attributed to the reducing strength of the Cl^- ion, particularly on heating, which is strong enough to oxidize Mn from its 4+ oxidation state to 2+. The green color of Cl_2 in solution is evident on digestion of the sample. In contrast, the SO_4^{2-} ion is an oxidizing agent but is not strong enough to oxidize Mn^{4+}.

In the study of a similarly prepared sample, Paik et al. showed that substantial extraction of Li was achieved by using 2.5 M H_2SO_4.[12] However, with the present as-prepared sample, the Li extraction with the 2.5 M acid was much less efficient. This is most likely due to a difference in particle size between the current Li_2MnO_3 and the previously reported samples.

X-ray Analysis. The powder X-ray diffraction pattern of the as-synthesized material is indicative of the Li_2MnO_3 structure. The structure of Li_2MnO_3 is layered, as shown in Figure 1, with a monoclinic unit cell and space group *C*2/*m*.[20,21] Figure 2 shows the Rietveld refinement fit of the X-ray

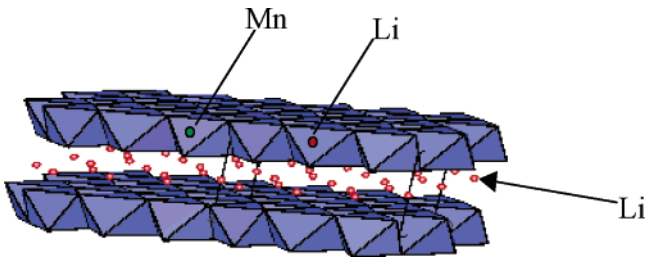

Figure 1. Layered structure of Li_2MnO_3.

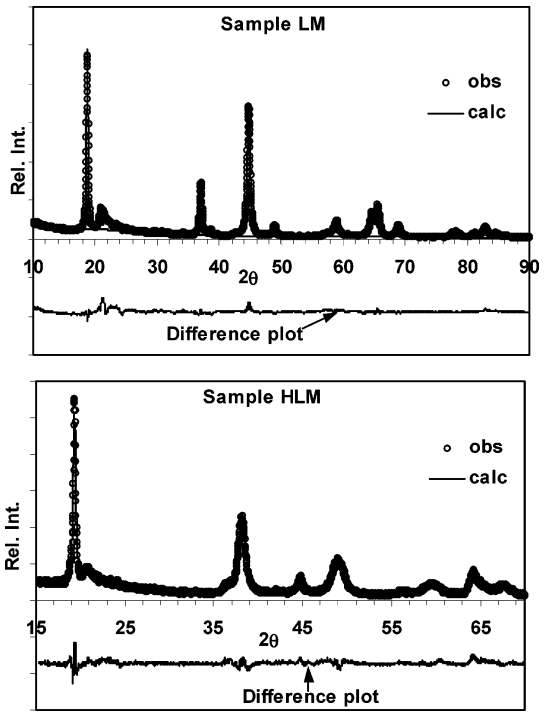

Figure 2. Rietveld refinement fits for the powder X-ray patterns for (a) sample LM and (b) the proton-exchanged sample HLM.

pattern that was performed using GSAS (general structure analysis system).[22] The obtained cell parameters are in good agreement with cell parameters, reported by Meng et al., that were obtained by the profile matching of synchroton data from a powder sample.[23] The obtained cell parameters are shown in Table 1. The presence of two types of cations, Li^+ and Mn^{4+}, in the transition metal layer that have a large difference in their charges causes cation ordering, which leads to the lowering of symmetry of the structure from $R\bar{3}m$ to *C*2/*m*. A prominent difference between these two symmetries is the peak at 2θ 21°, due to the superstructure, which is not present in a typical $R\bar{3}m$ XRD pattern. Earlier reports have discussed the lowering of symmetry.[12,24,25]

The acid treatment of the as-prepared material using 4.0 M H_2SO_4 at room temperature resulted in a phase change, as evidenced by the new peaks at the 2θ values of 38 and

(20) Strobel, P.; Lambert-Andron, B. *J. Solid State Chem.* **1988**, *75*, 1, 90.
(21) Massarotti, V.; Bini, M.; Capsoni, D.; Altomare, A.; Moliterni, A. G. *J. Appl. Crystallogr.* **1997**, *30*, 123.
(22) Larson, A. C.; Von Dreele, R. B. *General Structure Analysis System (GSAS)*; Los Alamos National Laboratory Report LAUR 86-748; Los Alamos National Laboratory: Los Alamos, NM, 2004.
(23) Meng, Y. S.; Ceder, G.; Grey, C. P.; Yoon, W.-S.; Jiang, M.; Breger, J.; Shao-Horn, Y. *Chem. Mater.* **2005**, *17*, 2386−2394.
(24) Rossouw, M. H.; Liles, D. C.; Thackeray, M. M. *J. Solid State Chem.* **1993**, *104*, 464.
(25) Robertson, A. D.; Bruce, P. G. *Chem. Mater.* **2003**, *15*, 1984−1992.

Table 1. Crystal Data for Samples LM and HLM

	LM	HLM	Li_2MnO_3[a]
space group	*C*2/*m*	*C*2/*m*	*C*2/*m*
cryst syst	monoclinic	monoclinic	monoclinic
a (Å)	4.940(1)	5.051(1)	4.9261(5)
b (Å)	8.527(1)	8.706(2)	8.527(1)
c (Å)	5.018(1)	4.904(1)	5.0280(7)
β (deg)	109.14(2)	109.19(2)	109.22(1)
cell volume (Å^3)	199.75(4)	203.70(6)	
D_{calcd} (g/cm^3)	3.89	3.30	
min/max 2θ (deg)	81	61	
no. of reflections	181	102	
R_{F2}	0.114	0.119	
R_{prof}	0.108	0.109	
wR_{prof}	0.149	0.136	
X-ray radiation wavelength, Cu Kα (Å)	1.5418	1.5418	
chemical formula	$Li_{1.33}Mn_{0.67}O_2$	$Li_{0.21}Mn_{0.67}O_{2.0}$	
Z	6	6	

[a] Previously reported data that was obtained from profile matching of Synchroton data.[24]

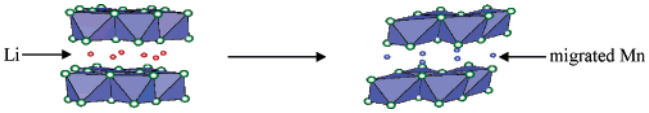

Figure 3. Layer shearing upon proton exchange.

49° and the shrinking of the peak at 45°. The new XRD pattern essentially matches that of a structure in the *R*3*m* symmetry, as for CrOOH. The structure of CrOOH consists of close-packed O atoms arranged in the "AABBCC" fashion, giving a *P*3 type structure. In the structure of CrOOH, the H atoms reside in trigonal prismatic sites, resulting in strong H-bonding. The retention of the peak at 21° 2θ upon acid treatment is due to monoclinic distortion of the *R*3*m* structure, which arises from cation ordering in the transition-metal layers. Rietveld refinement fit of the powder X-ray pattern of the proton-exchanged sample HLM, shown in Figure 2, conforms to the monoclinic structure in the *C*2/*m* symmetry. The geometry around the Mn is distorted octahedral. The corresponding *b*/*a* ratio and β values for sample HLM are 1.724 and 109.19°, respectively, which are consistent with monoclinic symmetry. The corresponding ideal values for rhombohedral symmetry are 1.732 and 109.14°. The peak broadening, upon H^+ exchange, increases with 2θ suggesting microstrain effect, which supports the presence of defects in the structure of sample HLM. As previously suggested, the refinement data supports layer shearing, as shown in Figure 3.[12]

As previously reported,[12] the sample shows a decrease in the *c* parameter upon Li extraction. As indicated in Table 1, proton exchange causes the *a* and *b* parameters to increase. This is consistent with protonation occurring within the main framework. The refinement data indicates the complete removal of all interlayer Li and partial delithiation from the main framework. The calculated chemical composition determined on the basis of the occupancies is $H_xLi_{0.21}Mn_{0.67}O_{2.0}$, which is in good agreement with the composition that was obtained from elemental analysis and titration. On the basis of the occupancies, there is indication of Mn migration from the main framework into the interlayer sites. When the refinement was performed with the assumption

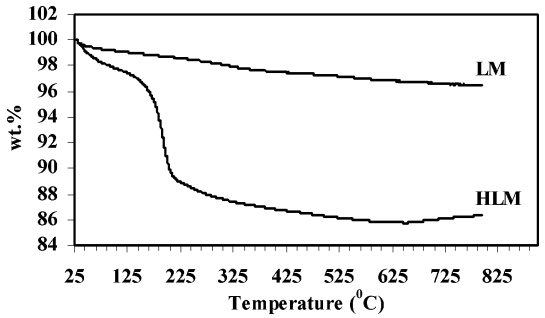

Figure 4. TGA profiles for the as-prepared sample and its H^+ form.

that the extra interlayer atoms were Li atoms, rather than Mn atoms, an unreasonably high Li:Mn ratio was obtained.

Thermal Analysis. The thermal behavior of Li_2MnO_3 and its proton-exchanged form has previously been reported.[12] The TGA profiles obtained for LM and HLM in O_2 are shown in Figure 4. X-ray analysis of the sample obtained by heating sample HLM to 600 °C indicates a mixture comprising mostly the spinel compound $LiMn_2O_4$ and Mn_2O_3, which points to the following decomposition reaction

$$H[H_{0.18}Li_{0.15}Mn_{0.67}]O_{1.90} \rightarrow 0.15LiMn_2O_4 + 0.19Mn_2O_3 + 0.59H_2O + 0.08O_2 \quad (4)$$

The calculated percentage weight change according to the eq 4 is 17.7%, which is reasonably close to the experimental percentage of 13.0%. The X-ray pattern (not shown) for the heated sample HLM shows evidence of extra peaks, of low intensity, which could not be identified. The presence of the extra phase explains the discrepancy between the calculated and experimental wt % loss. In the report by Paik et.-al., the material $H[Li_{0.33}Mn_{0.67}]O_3$ resulted only in $LiMn_2O_4$ as the decomposition product.[12] The difference in the decomposition products further supports the delithiation of sample LM from the transition-metal layers.

SEM and Surface Area Analyses. Images of the as-prepared sample LM and its H^+ form, obtained using a SEM technique, indicate a decrease in particle size upon proton exchange, as expected. The as-prepared sample LM shows particles of spherical morphology whose sizes are in the range 70−220 nm. The H^+ form sample HLM indicates average particle size in the range of 20−120 nm. Particles of sample HLM appear to be agglomerated, in contrast to those of sample LM. The prepared γ-MnOOH consists of needles of about 10 nm width and 500 nm length, as indicated in the SEM image in Figure 5. Surface area measurements, performed using the BET method, showed an increase in surface area upon acid treatment, consistent with SEM data. The obtained BET surface areas are 18 m^2/g for sample LM and 57 m^2/g for the sample HLM, whereas the surface area of the prepared γ-MnOOH was 36 m^2/g.

Electrochemistry. Cyclic voltammetry experiments were performed using sample mixtures consisting of the sample, carbon powder, and PTFE in a 4:1:1 mass ratio. The sample mixtures were coated on carbon papers. The experiments indicate that all the prepared samples reduce oxygen. Reduction peaks were obtained when O_2 was present. Upon deaeration of the cells with N_2, the reduction peaks disappeared.

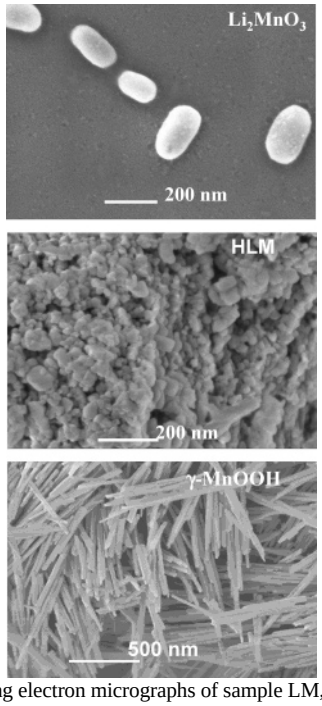

Figure 5. Scanning electron micrographs of sample LM, proton-exchanged sample HLM, and γ-MnOOH.

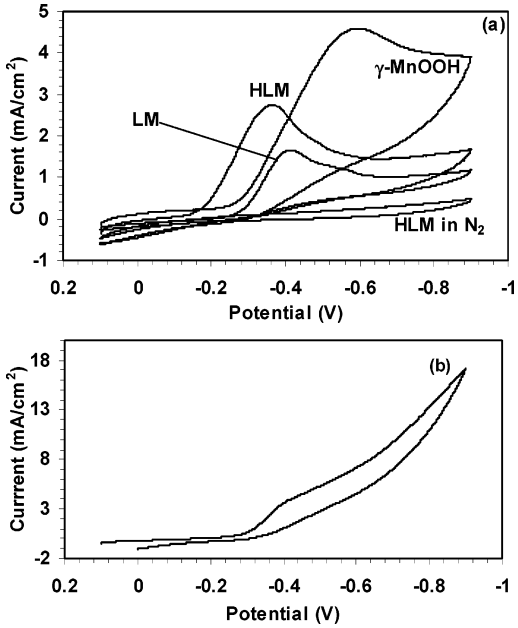

Figure 6. Cyclic voltammetry plots vs standard SCE obtained at a scan rate of 50 mV/s in 1 M KOH electrolyte for (a) samples LM, HLM, and γ-MnOOH in O_2 and HLM in N_2; (b) carbon powder and PTFE coated on carbon paper.

Figure 6 shows the voltammograms that were obtained using 1 M KOH electrolyte. Delithiation of the as-prepared sample LM results in an increase in the O_2 reduction ability. The increased surface area on the H^+ form contributes to the increased activity. Sample γ-MnOOH gives an O_2 reduction peak current that is higher compared to sample HLM. However, the reduction peak for sample HLM is at the most positive potential compared to the other two samples LM and γ-MnOOH. This is explained in terms of the presence of acidic protons in sample HLM, which facilitate a positive shift of the reduction potential. Although γ-MnOOH has H atoms in its structure like HLM, the protons in the latter are more acidic because of the presence of a higher Mn oxidation state (3.7+) than in the case of γ-MnOOH. The more positive O_2 reduction potential for HLM implies that if applied in an alkaline metal-air cell sample, HLM would give a relatively higher operational potential for the cell.

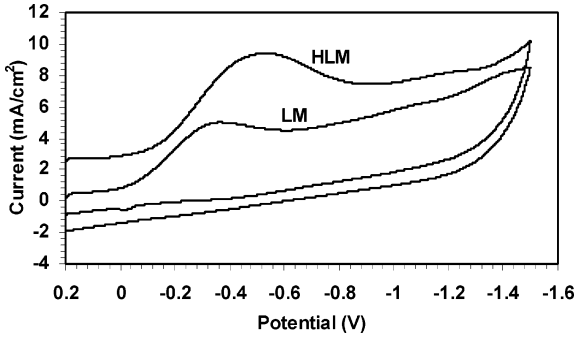

Figure 7. Cyclic voltammetry vs standard SCE for samples LM and HLM in organic electrolyte at a scan rate of 50 mV/s.

Both samples LM and HLM showed a restoration of the O_2 reduction peak when the electrolyte was repurged with O_2, indicating stability of the samples toward the O_2 reduction. The reduction peak potentials versus SCE for the samples are in the region expected for two-electron reduction[1] of O_2 as shown in eq 5

$$H_2O + O_2 + 2e^- \rightarrow HO_2^- + OH^- \qquad (5)$$

An experiment in which the sample was excluded while using carbon powder and PTFE alone gave no reduction peak in the scanned potential window.

Cyclic voltammetry of samples LM and HLM in an organic electrolyte, consisting of 1 M $LiPF_6$ in a mixture of DMC:EMC:EC, was studied in view of the potential application of the materials in Li-air batteries. Organic electrolyte is used in Li-air cells to avoid reaction between Li and H_2O.[26,27] Slightly higher O_2 reduction peak currents are obtained in the organic electrolyte, as shown in Figure 7, compared to KOH electrolyte. This is explained in terms of increased O_2 solubility in the organic electrolyte. The reduction potentials are in about the same region as for KOH electrolyte. However, there is a difference in the relative potentials for the reduction peaks of the two samples. The O_2 reduction potential for HLM is shifted about 0.1 V toward the more negative potential relative to the potential in KOH electrolyte. On the other hand, the reduction potential for sample LM is shifted about 0.1 V in the opposite direction. Clearly, there is a different type of electron-transfer process in play in the organic electrolyte compared to KOH electrolyte, which is not clear at this point.

When tested as electrocatalysts in Li-air cells, the samples gave discharge profiles as shown in Figure 8. Consistent with the CV data, a higher specific discharge capacity of 1618 mA h g^{-1} for sample HLM was obtained versus 1040 mA h g^{-1} for sample LM, at a current density of 0.15 mA/cm^2. For convention, the specific capacity is normalized to the weight of carbon. The specific capacity for sample HLM corresponds to an energy density of about 3721 mW h g^{-1}.

(26) Abraham, K. M.; Jiang, Z. *J. Electrochem. Soc.* **1996**, *143*, 1.
(27) Abraham, K. M.; Jiang, Z. U.S. Patent 5510209, 1996.

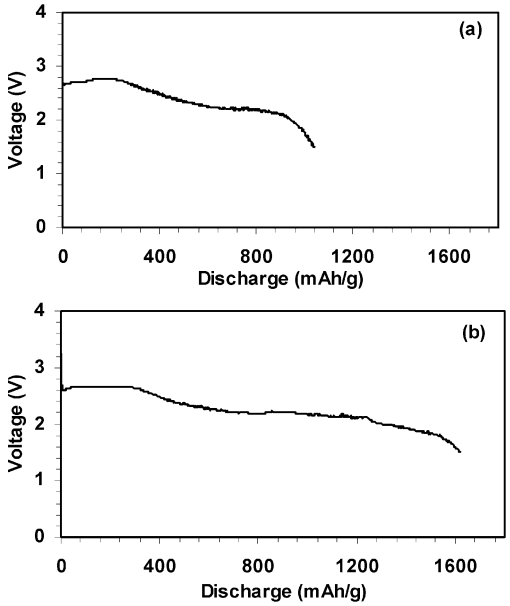

Figure 8. Discharge profiles for Li-air cells consisting of (a) sample LM and (b) sample HLM.

An experiment in which carbon alone was used as the electrocatalyst gave a specific capacity of about 1500 mA h g^{-1}. Earlier studies by Read gave a specific capacity of about 700 mA h g^{-1} when λ-MnO_2 was used as electrocatalyst in a Li-air cell consisting of 1 M $LiPF_6$ in PC:DME electrolyte, at a current density of 0.1 mA/cm^2.[28]

Conclusions

The layered Li_2MnO_3 (or $Li[Li_{0.33}Mn_{0.67}]O_2$), prepared by the reaction of γ-MnO_2 and LiOH, and its proton-exchanged form $H[H_{0.18}Li_{0.15}Mn_{0.67}]O_{1.90}$ show O_2 reduction abilities. The increased surface area of the H^+ form gives higher catalytic activity toward reduction of O_2, compared to sample LM. Sample HLM displays a more positive O_2 reduction potential relative to γ-MnOOH in KOH electrolyte. The acid-treated Li_2MnO_3 may therefore act as a good electrocatalyst in alkaline metal-air batteries. Analyses by ICP, average oxidation state determination, and titrations support the presence of O vacancies in the H^+ form. However, there is no evidence of the vacancies playing any significant role in its catalytic activity.

Oxygen reduction by the two samples LM and HLM in an organic electrolyte follows a different electron-transfer reaction than for KOH electrolyte. The reduction potentials due to HLM and LM are shifted toward the negative and positive directions, respectively, compared to the KOH electrolyte. In a Li-air cell, consisting of organic electrolyte, the delithiated sample HLM gives a specific capacity that is 50% higher than that of sample LM.

Acknowledgment. This work was funded by the Geo-Sciences and Biosciences Division, Office of Basic Energy Sciences and Office of Science, U.S. Department of Energy. We also thank Christine Morein and Abhay Vaze for their contributions in the electrochemical experiments.

Supporting Information Available: Crystallographic Information in CIF format; intensity vs 2θ plot for HLM after heating to 600°. This material is available free of charge via the Internet at http://pubs.acs.org.

CM0616937

(28) Read, J. *J. Electrochem. Soc.* **2002**, *149* (9), A1190−A1195.